Neutron spectroscopic factors of ^{34}Ar and ^{46}Ar from (p,d) transfer reactions

Jenny Lee (李曉菁),[1] M.B. Tsang (曾敏兒),[1] D. Bazin,[1] D. Coupland,[1] V. Henzl,[1] D. Henzlova,[1] M. Kilburn,[1] W. G. Lynch (連致標),[1] A. M. Rogers,[1] A. Sanetullaev,[1] Z. Y. Sun (孙志宇),[1,2] M. Youngs,[1] R. J. Charity,[3] L. G. Sobotka,[3] M. Famiano,[4] S. Hudan,[5] D. Shapira,[6] P. O'Malley,[7] W. A. Peters,[7] K. Y. Chae,[8] and K. Schmitt[8]

[1]*National Superconducting Cyclotron Laboratory & Department of Physics and Astronomy, Michigan State University, East Lansing, Michigan 48864, USA*

[2]*Institute of Modern Physics, CAS, Lanzhou 730000, China*

[3]*Department of Chemistry, Washington University, St. Louis, Missouri 63130, USA*

[4]*Department of Physics, Western Michigan University, Kalamazoo, Michigan 49008, USA*

[5]*Department of Chemistry, Indiana University, Bloomington, Indiana 47405, USA*

[6]*Oak Ridge National Laboratory, Oak Ridge, Tennessee 37831, USA*

[7]*Department of Physics and Astronomy, Rutgers University, Piscataway, New Jersey 08854, USA*

[8]*Department of Physics and Astronomy, University of Tennessee, Knoxville, Tennessee 37996, USA*

(Received 8 September 2010; published 27 January 2011)

Single-neutron-transfer measurements using (p,d) reactions have been performed at 33 MeV per nucleon with proton-rich ^{34}Ar and neutron-rich ^{46}Ar beams in inverse kinematics. The extracted spectroscopic factors are compared to the large-basis shell-model calculations. Relatively weak quenching of the spectroscopic factors is observed between ^{34}Ar and ^{46}Ar. The experimental results suggest that neutron correlations have a weak dependence on the asymmetry of the nucleus over this isotopic region. The present results are consistent with the systematics established from extensive studies of spectroscopic factors and dispersive optical-model analyses of $^{40-49}$Ca isotopes. They are, however, inconsistent with the trends obtained in knockout-reaction measurements.

DOI: 10.1103/PhysRevC.83.014606 PACS number(s): 25.40.Hs

I. INTRODUCTION

The asymmetry dependence of neutron correlations is essential in understanding properties of nuclei near the drip lines and of neutrons within neutron stars [1]. Unlike proton correlations, which have been observed to strengthen with neutron fraction in some regions of the nuclear chart [1,2], the dependence of neutron correlations on asymmetry is still under investigation [1,3]. These correlations do not occur in a pure mean-field description. Instead, residual interactions lead to the interplay between the single-particle and collective dynamics in a nucleus and result in the spread of the strength of a single-particle orbit over a large range in excitation energy [4]. The long-range component of the interaction, which induces couplings to the low-lying collective excitation and giant resonances, can be partly described in current shell models as configuration mixing near the Fermi surface by the residual interactions [4,5]. Many studies have made progress in exploring the details of the remaining long-range contributions as well as the short-range and tensor parts which are associated with the admixtures of high-momentum components [4,6].

The signatures of nucleon correlations are reflected in the fractional occupation of single-particle orbitals. This is quantified by the spectroscopic factor (SF), which probes the overlap between the many-body wave functions of the initial and final states of a transfer or knockout reaction [7]. Recent work has suggested that the quenching of spectroscopic factors is dominantly attributed to the long-range correlations [8]. To accurately determine the roles of the asymmetry dependence, one can study the spectroscopic factors for nuclei ranging from the valley of stability towards the drip lines. Large suppression (up to 75%) in spectroscopic-factor values compared to shell-model predictions for strongly bound valence nucleons has been observed in one-nucleon knockout reactions [9]. The cause of such huge asymmetry dependence, however, has not been explained. Furthermore, dispersive optical model (DOM) analyses, which include the effects of long-range correlations, indicate that the relative proton spectroscopic factor from ^{40}Ca to ^{49}Ca only changes by about 10% [3].

Extensive studies of consistent spectroscopic factors from single-neutron transfer using (p,d) and (d,p) reactions have been achieved recently by using systematic comparisons of cross-section data with angular distributions calculated in the adiabatic distorted wave approximation (ADWA) model [10,11]. In this work, the Johnson-Soper adiabatic three-body approximation [12] was employed via the code TWOFNR [13] to correct the deuteron breakup in the mean field of the target. If one adopts the Chapel-Hill nucleon-nucleus optical potential (CH89) [14] and a conventional Woods-Saxon potential of fixed radius $r_0 = 1.25$ fm and diffuseness $a_0 = 0.65$ fm, one finds better than 20% agreement between experimental measurements and the predictions from large-basis shell-model (LB-SM) calculations of ground-state and most excited-state neutron spectroscopic factors for stable nuclei with $3 \leqslant Z \leqslant 28$ [15,16]. On the other hand, the measured ground-state spectroscopic factors are suppressed by about 30% compared to LB-SM predictions for most nuclei [17] if the ADWA reaction model uses the JLM potential developed by Jeukenne, Lejeune, and Mahaux [18] with the conventional scale factors for the computed real and imaginary part of $\lambda_V = 1.0$ and $\lambda_W = 0.8$ [19] and if one constrains the geometry of the potential and the transferred-neutron bound state with Hartee-Fock calculations [20]. This suppression

is similar to that observed for the proton spectroscopic factors obtained in $(e,e'p)$ measurements near the closed shells, where the absolute proton spectroscopic factor values are reduced systematically by 30%–40% compared to the independent-particle model [21]. Independent of the choice of optical model potentials and geometries of the bound-neutron wave functions, the comprehensive data obtained from single-neutron transfer reactions suggest the reduction factor *Rs* (the ratio of experimental spectroscopic factor to prediction) is independent of the neutron binding energy for stable nuclei within experimental uncertainties [11]. This suggests that there are no strong neutron correlation effects on the asymmetry of the nucleus. However, the uncertainties in these systematic studies are somewhat large, because the data were gleaned from various experiments performed over the past four decades, each with its own systematic uncertainty. In addition, the compiled reactions include very few nuclei with extreme isospin composition.

To explore the regions of extreme N/Z, (p,d) neutron transfer reactions have been studied using proton-rich ^{34}Ar and neutron-rich ^{46}Ar beams in inverse kinematics to extract the experimental neutron spectroscopic factors for ^{34}Ar and ^{46}Ar. Some of the results have been published in Ref. [22]. The present article provides a detailed report of the experimental measurements and results presented in Ref. [22].

II. EXPERIMENTAL SET UP

Measurements of angular distributions for $p(^{34}\text{Ar},d)^{33}\text{Ar}$, $p(^{36}\text{Ar},d)^{35}\text{Ar}$, and $p(^{46}\text{Ar},d)^{45}\text{Ar}$ reactions were performed at the National Superconducting Cyclotron Laboratory at Michigan State University. Primary beams of ^{36}Ar and ^{48}Ca were accelerated by the Coupled-Cyclotron Facility (CCF) [23] where secondary beams are produced using the in-flight projectile fragmentation technique. A secondary ^{34}Ar beam was produced by impinging the 150-MeV/nucleon ^{36}Ar primary beam on a 1480-mg/cm^2 ^{9}Be production target. The ^{46}Ar beam was produced by impinging the 140-MeV/nucleon ^{48}Ca beam on a 1763-mg/cm^2 ^{9}Be production target. After fragmentation, the radioactive beams were selected by the A1900 large-acceptance fragment separator [24]. A 375-mg/cm^2-thick achromatic aluminum wedge degrader and momentum slits at the dispersive image of the separator were employed to degrade the beams to 33 MeV per nucleon and further purify the beams, resulting in ^{34}Ar and ^{46}Ar beams with average purities of 94% and ∼100%, respectively. The ^{34}Ar and ^{46}Ar beams were identified unambiguously using the measured time of flight from the cyclotron to the A1900 focal plane. To check the current experimental method against previous measurements in normal kinematics [25], reactions with ^{36}Ar primary beam degraded to 33 MeV/nucleon were performed.

Beams were focused on a CH_2 target in the S800 chamber. Targets with thicknesses of 7.10 mg/cm^2 for the $p(^{34,36}\text{Ar},d)^{33,35}\text{Ar}$ reactions and 2.29 mg/cm^2 for the $p(^{46}\text{Ar},d)^{45}\text{Ar}$ reaction were used. The target thickness was chosen by finding a compromise between maximizing the transfer reaction yields and minimizing the energy loss and angular and energy loss straggling of deuterons in the target. To assess background contributions from the reactions with C nuclei, reactions on a 17-mg/cm^2-thick uniform carbon target were measured.

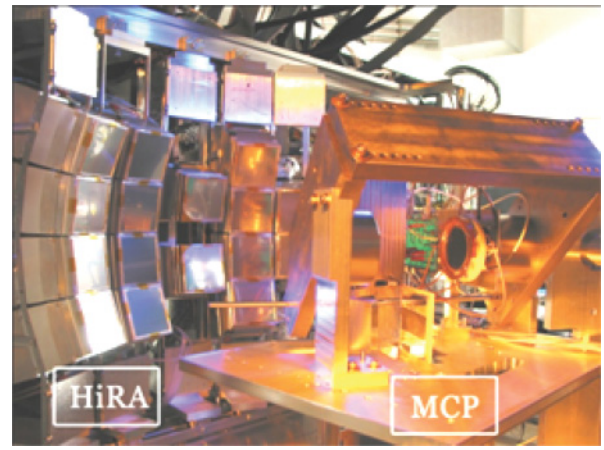

FIG. 1. (Color online) Experimental setup of HiRA and MCP.

The experimental setup relevant to the results reported here is shown in the photograph in Fig. 1. For complete kinematic reconstruction of the reactions, the high-resolution silicon array (HiRA) [26] was used to measure the energies and angles of the emitted deuterons while the coincident recoil residues were detected by the S800 spectrometer [27,28] located behind the chamber (not shown in the photograph). One multichannel plate (MCP) detector [29,30], placed approximately 10 cm upstream of the target, was used to monitor the absolute beam intensities throughout the experiment.

In the setup, 16 HiRA telescopes were arranged in 5 towers located 35 cm downstream from the target. These telescopes subtended polar angles of 4°–45° in the laboratory. The gap at angles less than 4 degrees allowed heavy reaction fragments to reach the S800 spectrometer. The beam was able to pass through the gap without hitting the telescopes. Each HiRA telescope consists of a ΔE (65 μm) and an E (1500 μm) silicon strip detector backed by four separate CsI(Tl) crystals arranged to cover the four quadrants of the silicon detectors. Each silicon detector has an active area of 6.25 cm × 6.25 cm, subdivided into 32 position-sensitive strips in the single-sided ΔE detectors and into $32 \times 32 = 1024$ pixels for the double-sided E detectors. The 2-mm pitch of these strips provided an angular resolution of ±0.16°, which is necessary to achieve good energy resolution in constructing the Q-value spectra. Due to the forward focusing of the deuterons, this setup covers most of the relevant solid angle for all three reactions. The average geometrical efficiency is about 30% over the relevant angular domain.

Figure 2 shows the actual geometric efficiency of 16 HiRA telescopes when the two middle strips in both front and back sides of the E silicon detectors as well as any nonfunctioning CsI(Tl) crystals and silicon strips are excluded. The middle strips, which cover the gaps between the four separated CsI crystals, are discarded in the analysis to ensure that all the particles punching through the silicon detector hit a well-defined CsI that is unambiguously given by the silicon quadrant. Rejecting high-energy particles that punch through to the CsI detectors improves the particle identification of

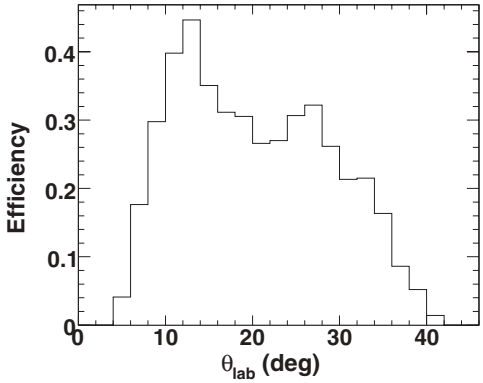

FIG. 2. Geometry efficiency in laboratory frame for detection of the deuterons in the HiRA (see text).

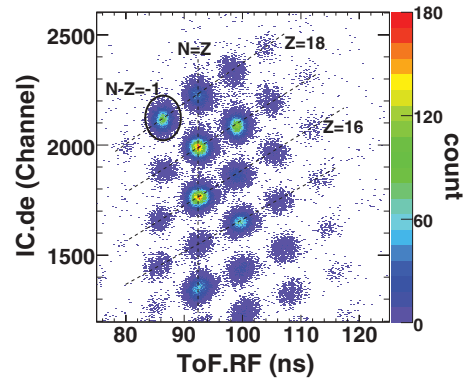

FIG. 4. (Color online) S800 particle identification spectrum for the $p(^{36}\mathrm{Ar},d)$ reaction. The reaction residue of interest, ^{35}Ar, is circled (see text).

the deuteron particles that stop in the E Si detectors. More detailed descriptions of the HiRA telescopes and the current experimental setup can be found in Refs. [26,31].

To ensure excellent energy and angular resolutions, the position of every pixel relative to the target was determined to sub-mm accuracy using the laser-based alignment system (LBAS). An accuracy of approximate 0.3 mm, which corresponds to 0.05° in the alignment of the detectors and the reaction target, was achieved. Details about operation of the LBAS are given in Refs. [31,32].

III. EXPERIMENTAL RESULTS

A. Kinematics reconstruction

Charged particles emitted in the reactions are detected by HiRA. Good particle identifications for hydrogen and helium isotopes are achieved using the energy detected in the ΔE (65 μm) and E (1.5 mm) silicon detectors and CsI detectors. Figure 3 shows a two-dimension plot of DE, the energy loss in the ΔE detector, vs. EF, the energy of the stopped particles deposited in the E detector for the particles. Rejecting punch-through particles reduced the background and allowed very clear identification of particles all the way up to the punch-though energy of protons, deuterons, and tritons.

The reaction residues in the S800 were identified using the energy loss in the ionization chamber (IC.de) and their time-of-flight signals using the cyclotron RF frequency as a reference (ToF.RF) [27,28]. An example of the S800 particle identification for the $p(^{36}\mathrm{Ar},d)^{35}\mathrm{Ar}$ reaction is shown in Fig. 4. The circle indicates the gate of residue ^{35}Ar. The large momentum acceptance (>5%) of S800 spectrometer allows the measurements of all the residues of interest from the three reactions $p(^{34,36,46}\mathrm{Ar},d)^{33,35,45}\mathrm{Ar}$. By measuring both outgoing particles (i.e., "complete kinematics"), the background and random-coincidence contributions are reduced to negligible levels, as verified by the measurements with the carbon target.

For the coincidence events, the reaction kinematics were determined from the energy and angle of the detected deuteron on an event-by-event basis. Figure 5 is a typical inverse kinematic plot of (p,d) reactions showing the energy of deuterons (E_d) in the laboratory frame gated on the beams and recoil residues from $p(^{34}\mathrm{Ar},d)^{33}\mathrm{Ar}$ reactions. The curves in the spectrum are the calculated kinematics corresponding to the excitation energies of 0, 1.359, 1.798, 3.456, and 3.819 MeV for the reaction residues ^{33}Ar as compiled in the National Nuclear Data Center (NNDC) database [33]. Figure 5 shows the large kinematic broadening at backward angles where corrections of beam angle and precise location of the

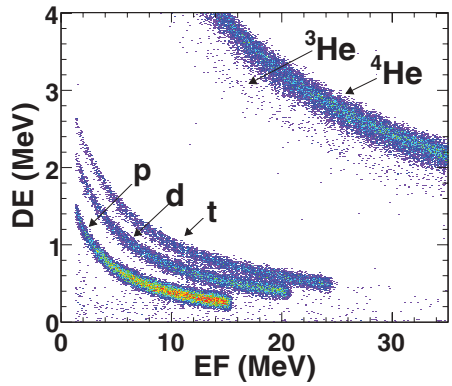

FIG. 3. (Color online) Particle identification for hydrogen and helium isotopes in the HiRA (see text).

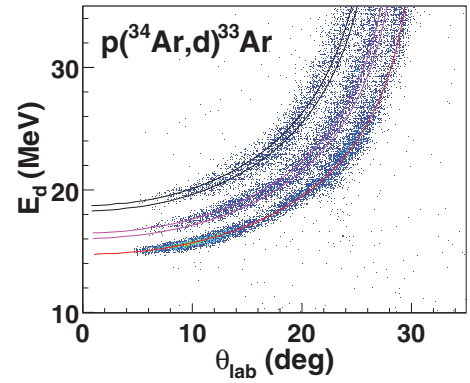

FIG. 5. (Color online) Deuteron kinematics for $p(^{34}\mathrm{Ar},d)^{33}\mathrm{Ar}$ in the laboratory frame (see text).

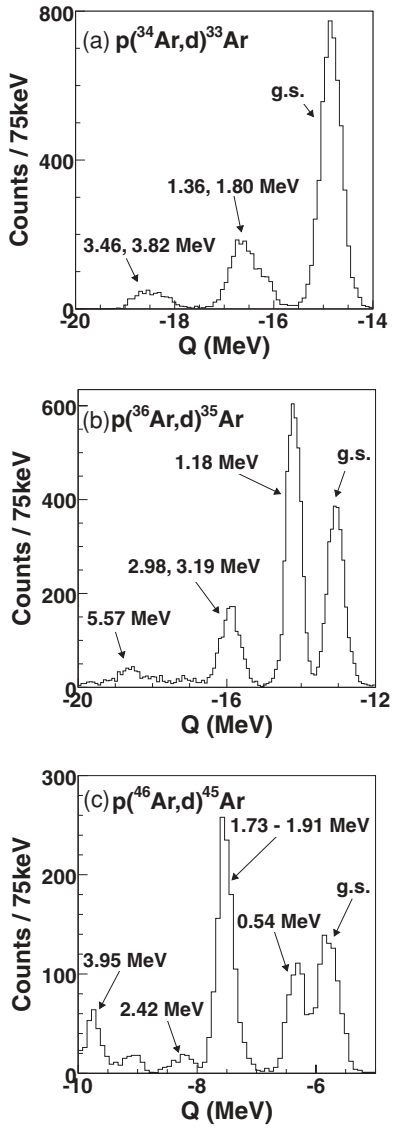

FIG. 6. Q-value spectra for (a) $p(^{34}\mathrm{Ar},d)^{33}\mathrm{Ar}$, (b) $p(^{36}\mathrm{Ar},d)^{35}\mathrm{Ar}$, and (c) $p(^{46}\mathrm{Ar},d)^{45}\mathrm{Ar}$.

reaction become important in order to resolve closely spaced states.

The deduced reaction Q-value spectra for $p(^{34}\mathrm{Ar},d)^{33}\mathrm{Ar}$, $p(^{36}\mathrm{Ar},d)^{35}\mathrm{Ar}$, and $p(^{46}\mathrm{Ar},d)^{45}\mathrm{Ar}$, based on missing-mass analyses, are shown in Fig. 6. Since most of the deuterons of interest stop in the Si detectors, the Q-value spectra presented here exclude events in which the deuterons punch though the thick Si detector. The energy resolution of the CsI crystals is worse than that of the Si detectors. Only deuterons with energy greater than 22 MeV emitted mainly at backward angles are detected by the CsI detectors. The excitation energies of a number of low-lying states were identified as indicated in the Q-value spectrum. The excitation energies are taken from the Nuclear Science References (NSR) database of the NNDC [33].

For $p(^{34}\mathrm{Ar},d)^{33}\mathrm{Ar}$, the peak in the Q-value spectrum in Fig. 6(a) corresponding to the ground-state transition is well distinguished. The next peak at higher excitation energy is comprised of the first two excited states (1.358 MeV and 1.798 MeV [33]). In the Q-value spectrum for the $^{36}\mathrm{Ar}$ target [Fig. 6(b)], the ground state and the first-excited state at 1.184 MeV [33] are clearly identified. The Q-value spectrum for the $^{46}\mathrm{Ar}$ target [Fig. 6(c)] covers laboratory angles up to about 19°, where kinematic broadening is minimized. The ground state and first-excited state (0.542 MeV) at larger angles could not be resolved completely.

The energy resolution of the ground-state peaks in the Q-value spectra was verified with GEANT4 simulations [34]. The simulations take into account the performance of HiRA detectors, angular and energy straggling, kinematics broadening, as well as the energy resolution of the beam and the finite size of the beam spot. The observed resolutions of approximately 500, 470, and 416 keV full width at half maximum (FWHM) for the ground-state transitions of $^{34}\mathrm{Ar}$, $^{36}\mathrm{Ar}$, and $^{46}\mathrm{Ar}$ are consistent with the predicted resolutions from simulations of 495, 420, and 377 keV, respectively [31]. The main contributions to the resolutions are the target thickness and the kinematic dispersion due to the large beam spots. Ability to correct the incident beam positions and angles should improve the resolution, which is important for the excited states. A detailed analysis of the excited states with improved resolution will be discussed in a forthcoming article [35].

B. Absolute cross-section measurements

The beam intensities were continuously monitored with the MCP [29,30] detection system placed 10 cm upstream from the reaction target. Absolute normalizations are determined by taking into account the live time of data acquisition, the individual detector efficiencies, and the detection coverage. To estimate the overall normalization uncertainties arising from the systematic uncertainty attributed to the detector efficiencies and lifetime of the data-acquisition (DAQ) system, we calculated the cross section corresponding to approximately every successive 100 counts detected in a 2-degree bin in the region of peak cross section for each reaction. Figure 7 shows the cross sections extracted from these groups at deuteron angles of $\theta_{\mathrm{lab}} = 9°$ for $p(^{34}\mathrm{Ar},d)^{33}\mathrm{Ar}$, $\theta_{\mathrm{lab}} = 23°$ for $p(^{36}\mathrm{Ar},d)^{35}\mathrm{Ar}$, and $\theta_{\mathrm{lab}} = 15°$ for $p(^{46}\mathrm{Ar},d)^{45}\mathrm{Ar}$ reactions denoted by open circles, closed circles and solid squares respectively. The solid lines indicate the cross sections extracted using all the available data. Small fluctuations are observed and the large deviations in the second and third data group of $p(^{46}\mathrm{Ar},d)^{45}\mathrm{Ar}$ can be explained by the unstable performance of the MCP detectors during those runs. The standard deviations are 7.5% for $^{36}\mathrm{Ar}$, 6.3% for $^{34}\mathrm{Ar}$, and 5.7% for $^{46}\mathrm{Ar}$. Based on this analysis, we adopt an overall uncertainty of 8% for all the spectroscopic factors we extracted, as described in the next section. Detailed procedures and discussions about the determination of absolute normalization can be found in Ref. [31].

The reaction $^{36}\mathrm{Ar}(p,d)^{35}\mathrm{Ar}$ has been studied previously in normal kinematics by Kozub *et al.* [25] at 33.6 MeV/nucleon. The angular distributions for the inverse kinematics reaction $p(^{36}\mathrm{Ar},d)^{35}\mathrm{Ar}$ for transitions to ground and first-excited states measured in the present study at 33 MeV/nucleon are

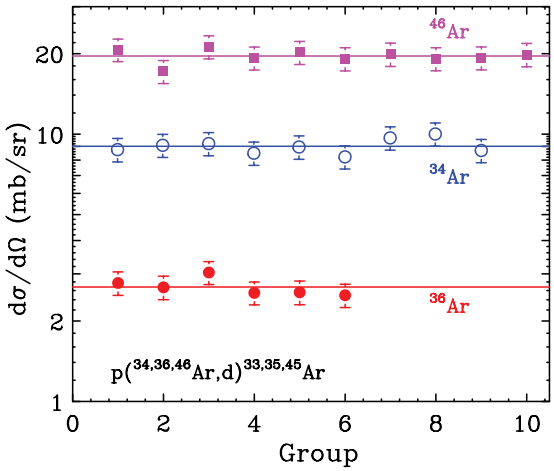

FIG. 7. (Color online) Comparisons of peak absolute differential cross sections for successive measurements taken over the entire experiment. The open circles, closed circles and solid squares denote results of $p(^{34}\mathrm{Ar},d)$, $p(^{36}\mathrm{Ar},d)$ and $p(^{46}\mathrm{Ar},d)$ reactions respectively (see text).

compared to the previous work of Ref. [25] in the top and bottom panels of Fig. 8, respectively. In Fig. 8, our data are denoted by closed circles and the results of Ref. [25] are denoted as open squares. The error bars given in Ref. [25] are most likely statistical errors and are smaller than the size of the symbols. The differential cross sections from Ref. [25] and from the present measurement are in reasonable agreement.

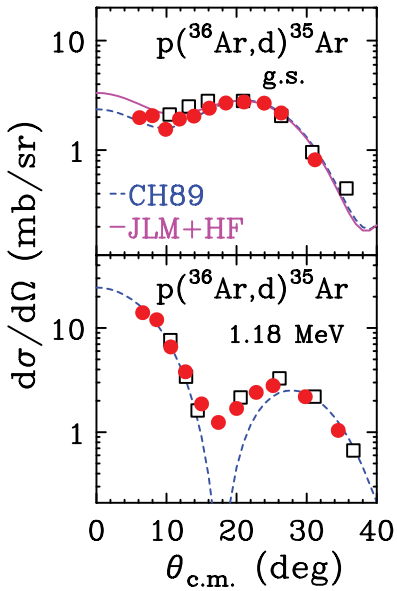

FIG. 8. (Color online) (Top) Differential cross sections for $p(^{36}\mathrm{Ar},d)^{35}\mathrm{Ar}$ in the center-of-mass frame for the ground-state transition. (Bottom) Differential cross sections for the first-excited state (1.18 MeV). Circles and squares denote our results and previous measurements in Ref. [25], respectively. Curves are the predicted angular distributions multiplied by the spectroscopic factors. Solid and dash lines represent the calculations with parameters of CH89 and JLM + HF approaches.

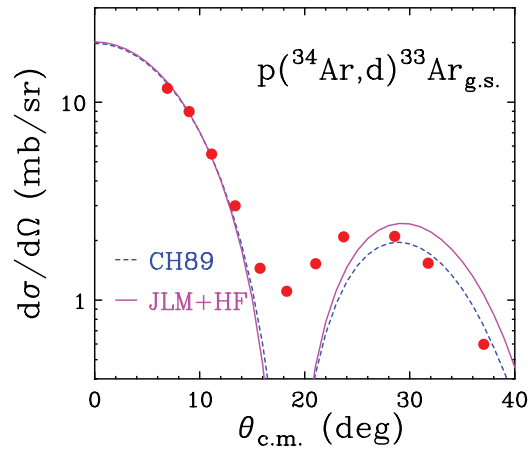

FIG. 9. (Color online) Differential cross sections for $p(^{34}\mathrm{Ar},d)^{33}\mathrm{Ar}$ in the center-of-mass frame for the ground-state transition. Curves are the predicted angular distributions multiplied by the spectroscopic factor. Solid and dash lines represent the calculations with parameters of CH89 and JLM + HF approaches.

C. Angular distributions and ground-state spectroscopic factors

In this section, the experimental differential cross sections for transitions to the ground states are compared to ADWA calculations. Two different input parameter sets for the ADWA calculations are used to predict the angular distributions: (a) CH89 global optical-model potentials and a fixed radius parameter of 1.25 fm for Woods-Saxon geometry for the orbital of the transferred neutron [11,15] and (b) JLM optical potentials and geometry for transferred neutron constrained by Hartree-Fock calculations [17]. At present, approach (b) can only be used to predict the angular distributions of the ground state since HF calculations for the nucleon densities and the radii of transferred nucleons in the excited states are not available. Unless indicated otherwise, the experimental uncertainties associated with the extracted spectroscopic data shown in this section come from statistical and systematic uncertainties. In most cases, they are about 8%, as discussed in the previous section.

To follow the convention of Ref. [15,17], we labeled the two reaction model parameter sets as "CH89" and "JLM + HF," respectively. Calculations plotted in Figs. 8, 9, and 10 are normalized to the data around the first maximum [11]. Angular distributions and spectroscopic factors for each reaction are discussed in the following subsections.

$p(^{34}\mathrm{Ar},d)^{33}\mathrm{Ar}$

For $p(^{34}\mathrm{Ar},d)^{33}\mathrm{Ar}$, the shapes of the predicted angular distributions from CH89 (dashed curve) and JLM + HF (solid curve) are in reasonable agreement with the data for the ground-state transition shown in Fig. 9. The agreement with the first peak, which determines the spectroscopic factors, is especially good. The forward peaking of the angular distribution clearly characterizes the $l = 0$ angular momentum transfer in the reaction. SF(CH89) $= 1.1 \pm 0.09$ and SF(JLM + HF) $= 0.85 \pm 0.06$ were extracted by using the first three

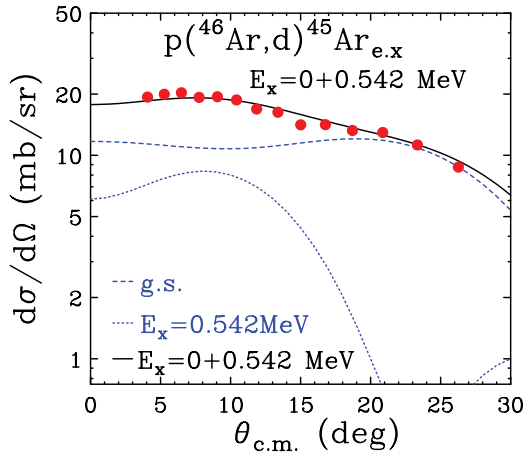

FIG. 10. (Color online) Differential cross sections of $p(^{46}\mathrm{Ar},d)^{45}\mathrm{Ar}$ in center-of-mass frame for transitions to ground state and first-excited state. Curves are the predicted angular distributions multiplied by the spectroscopic factor (see text).

data points.

$$p(^{36}\mathrm{Ar},d)^{35}\mathrm{Ar}$$

As shown in Figure 8, the calculated deuteron angular distributions from $p(^{36}\mathrm{Ar},d)^{35}\mathrm{Ar}$ reactions using CH89 approaches describe both sets of data leading to the ground-state and first-excited-state transitions of $^{35}\mathrm{Ar}$ very well. Calculations using JLM + HF approaches describe the ground-state transition data reasonably well. The CH89 method reproduces the cross sections of the ground-state transition better at the very forward angles. For the ground-state transition, the six points in the first peak were used to obtain spectroscopic factors, and the extracted values are SF(CH89) = 2.3 ± 0.2 and SF(JLM + HF) = 1.6 ± 0.1. For the first excited state, the first three points were used to obtain SF(CH89) = 1.2 ± 0.1. No JLM + HF calculation was performed for the excited states.

$$p(^{46}\mathrm{Ar},d)^{45}\mathrm{Ar}$$

For the $p(^{46}\mathrm{Ar},d)^{45}\mathrm{Ar}$ reaction, the peaks for the ground state and first-excited state of $^{45}\mathrm{Ar}$ are separated by 0.542 MeV [33]. Due to the severe kinematical broadening for these reactions at large angles and the lack of beam-tracking ability in the analysis, we did not completely resolve the ground-state and first-excited-state transitions at all angles. Figure 10 shows the experimental data contributed by both the ground- and first-excited-state transitions. In Ref. [22], the distinct $l = 3$ and $l = 1$characteristics for the ground- and first-excited-state transition are used to determine their individual contributions to the ground-state differential cross sections for center-of-mass angles less than 8° and between 20° to 27°. The dashed and dotted lines in Fig. 10 represent the angular distributions of $l = 3$ ground-state and $l = 1$ first-excited-state transitions, and the solid line is the total angular distributions. All the data points are used for two-l-value fitting constrained by the respective SF extracted at small angles. In general, the shape of the experimental data is reasonably reproduced, and the resulting SF(CH89) for ground state is 5.08 ± 0.4. This value is consistent with 5.28 ± 0.4 obtained in Ref. [22].

D. Asymmetry dependence of reduction factors

The LB-SM calculations for $^{33,35}\mathrm{Ar}$ were performed using the code OXBASH [36] in an *sd* shell-model space with the USDB interaction [37]. For $^{46}\mathrm{Ar}$, the interaction of Nummela *et al.* in an *sdpf* shell-model space was used [38,39]. The ground-state values for *Rs*, the ratio of experimental to theoretical spectroscopic factors, were deduced for the two reaction parameter sets involving the CH89 or JLM + HF parameters, as described in Sec. III C. The results for symmetric $^{36}\mathrm{Ar}$ and neutron-rich $^{46}\mathrm{Ar}$ are similar, with no quenching observed. This is consistent with the previous systematic studies with stable nuclei [11,15]. The extracted value of ground-state *Rs* for proton-rich $^{34}\mathrm{Ar}$ is about 15%–20% smaller than those of $^{36}\mathrm{Ar}$ and $^{46}\mathrm{Ar}$, which is within the uncertainties of the systematics.

The theoretical and the experimental SFs from transfer reactions for stable Ar isotopes were published in Ref. [11], where LB-SM calculations use the USDB interaction [37] in the *sd* shell-model space for $^{37-38}\mathrm{Ar}$ isotopes and the SDPFNOW interaction [39] in the *sdpf* shell-model space for $^{39-41}\mathrm{Ar}$. To show the asymmetry dependence of the chain of Ar isotopes, reduction factors of all the Ar nuclei obtained from the present experiments (solid circles) and from previous measurements (solid stars) [11] are shown in Fig. 11. They are plotted as a function of ΔS, which characterizes the asymmetry dependence of the relative shift of the neutron and proton Fermi surfaces. For simplicity, only *Rs* values deduced from the JLM + HF parameter set are presented. A similar trend is observed for *Rs* (CH89). The ΔS values of $^{46}\mathrm{Ar}$ and $^{34}\mathrm{Ar}$ are −10.03 and 12.41 MeV, respectively, significantly increasing the span of the separation energy difference from the previous transfer reaction data on stable isotopes. In previous studies, there were no nuclei with $\Delta S \gg 7$ MeV [15,17].

In Fig. 11, the error bars for $^{38}\mathrm{Ar}$ are larger than the others because there is only one measurement available and no other independent measurement exists for a consistency check [40]. In the case of $^{40}\mathrm{Ar}$, which is not included in the figure, there are two sets of measurements. However, the extracted SFs from the two experiments are different by about

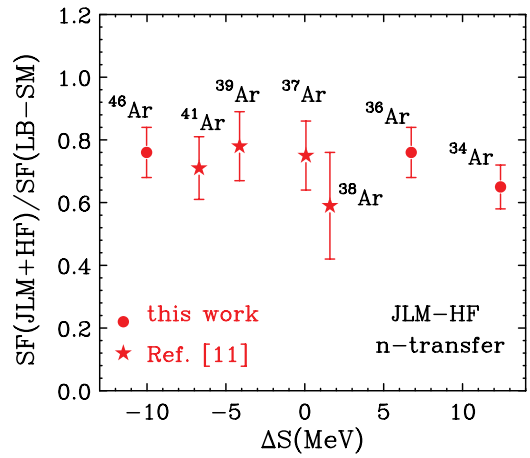

FIG. 11. (Color online) The ground-state reduction factors deduced using JLM-HF approach SF(JLM-HF)/SF(LB-SM) of the proton-rich $^{34}\mathrm{Ar}$ and neutron-rich $^{46}\mathrm{Ar}$, together with the symmetric $^{36}\mathrm{Ar}$ and the well-bound $^{37-41}\mathrm{Ar}$ isotopes [11].

a factor of 2, possibly due to problems in obtaining the absolute cross sections [41,42]. Within experimental uncertainties, little suppression in the reduction factor is found for proton-rich ^{34}Ar compared with the well-bound nuclei or neutron-rich ^{46}Ar. Such weak dependence on asymmetry is not consistent with the trends observed from knockout reactions [22] where the neutron *Rs* of ^{34}Ar is smaller by a factor of 2 compared with the *Rs* of ^{46}Ar [9]. This suggests that a reassessment of the approximations used in the theoretical treatment of transfer reactions and of knockout reactions may be necessary. Full three-body Faddeev calculations have been performed to evaluate possible theoretical errors from three-body effects in the transfer reaction in Ref. [43]. These calculations provided an estimate of about 20% for the theoretical uncertainty in the extracted SFs arising from various approximations in the reaction model [43]. A similar assessment for knockout reaction calculations would be useful.

This weak dependence of reduction factors on the asymmetry indicates a weak dependence of valence neutron correlations on the asymmetry of Argon isotopes. Similar conclusion can be drawn from the overall trends for spectroscopic factors extracted from systematic transfer reaction studies [11,15]. It is interesting to compare these results to the trends reported for valence protons extracted from dispersive optical model (DOM) analyses [2,3]. The recent DOM analysis of elastic-scattering and bound-level data for $^{40-49}$Ca isotopes suggests that the proton correlations also exhibit weak dependence on the asymmetry; there, the ground-state proton SF magnitude from ^{40}Ca to ^{48}Ca changes by about 10% [2,3]. Clearly, greater sensitivity of the asymmetry dependence of proton and neutron correlations can be achieved by extending transfer reaction and DOM studies towards the proton and neutron drip lines in different mass regions of the nuclear chart. Based on both analyses, careful measurements may be required if the effects remain at the 10%–20% level as our study and the DOM studies suggest.

IV. CONCLUSIONS

In summary, we have extracted the neutron ground-state spectroscopic factors of proton-rich ^{34}Ar, neutron-rich ^{46}Ar, and stable ^{36}Ar nuclei using (p,d) transfer reactions with radioactive beams in inverse kinematics. The complete-kinematics measurements were achieved using the high-resolution silicon array HiRA to measure the deuterons in coincidence with the recoil residues detected in the S800 mass spectrometer. The deuteron differential cross sections obtained in the experiments are compared to theoretical cross sections calculated using both (a) Chapel-Hill (CH89) nucleon-nucleus global optical potential with neutron potentials of fixed radius and diffuseness parameters and (b) JLM potential from Jeukenne, Lejeune, and Mahaux with the geometry of the potential and the transferred-neutron bound state constrained by Hartee-Fock calculations. Experimental neutron spectroscopic factors are extracted and compared to the predictions from large-basis shell models. Consistent with previous systematic studies with stable nuclei, the reduction factors for symmetric ^{36}Ar and neutron-rich ^{46}Ar are similar. The extracted reduction factor for proton-rich ^{34}Ar is about 15%–20% smaller. With the experimental uncertainties of $\pm$8%, reductions in the spectroscopic factors for proton-rich ^{34}Ar relative to neutron-rich ^{46}Ar of 0%–35% are possible but much larger reductions are excluded. The weak dependence of reduction factors on the asymmetry of the three Ar isotopes is similar to the trends obtained from the recent dispersive-optical-model analysis of elastic-scattering and bound-level data for $^{40-49}$Ca isotopes. In the latter study, the experimental trend is consistent with no or weak asymmetry dependence in the neutron correlations for $N > Z$ Ca isotopes. In the same analysis, the proton spectroscopic factor from ^{40}Ca to ^{48}Ca has a weak (10%) dependence on the asymmetry.

In single-nucleon knockout reactions at intermediate energies, the deficient nucleon species appear to have stronger reductions in their spectroscopic factors than the weakly bound excess species. In particular, the extracted neutron reduction factor of ^{34}Ar is smaller by a factor of 2 compared with that of ^{46}Ar. Unlike the trends observed for knockout reactions, comparison of the extracted spectroscopic factors for proton-rich ^{34}Ar and neutron-rich ^{46}Ar using transfer reactions suggests a weak dependence of correlations on neutron-proton asymmetry in this isotope region. The origin of such a discrepancy between the spectroscopic factors extracted from transfer and knockout reactions is not clear. The new results pose an intriguing question about the reaction mechanisms of transfer and knockout reactions as well as the nature of neutron correlations in nuclei with extreme isospin asymmetry. Further theoretical study would be needed to resolve the inconsistency in the reaction mechanisms and better describe the asymmetry dependence of nucleon correlations in nuclei away from the valley of stability towards the drip lines.

[1] T. Frick, H. Muther, A. Rios, A. Polls, and A. Ramos, Phys. Rev. C **71**, 014313 (2005).
[2] R. J. Charity, L. G. Sobotka, and W. H. Dickhoff, Phys. Rev. Lett. **97**, 162503 (2006).
[3] R. J. Charity, J. M. Mueller, L. G. Sobotka, and W. H. Dickhoff, Phys. Rev. C **76**, 044314 (2007).
[4] W.H. Dickoff and C. Barbieri, Prog. Part. Nucl. Phys. **52**, 377 (2004).
[5] B. A. Brown, Prog. Part. Nucl. Phys. **47**, 517 (2001).
[6] V. R. Pandharipande *et al.*, Rev. Mod. Phys. **69**, 981 (1997).
[7] N. Austern, *Direct Nuclear Reaction Theories* (John Wiley & Sons, New York, 1970).
[8] C. Barbieri, Phys. Rev. Lett. **103**, 202502 (2009).
[9] A. Gade *et al.*, Phys. Rev. C **77**, 044306 (2008), and references therein.
[10] X. D. Liu, M. A. Famiano, W. G. Lynch, M. B. Tsang, and J. A. Tostevin, Phys. Rev. C **69**, 064313 (2004).
[11] J. Lee, M. B. Tsang, and W. G. Lynch, Phys. Rev. C **75**, 064320 (2007), and references therein.
[12] R. C. Johnson and P. J. R. Soper, Phys. Rev. C **1**, 976 (1970).

[13] M. Igarashi, M. Toyoma, and N. Kishida, *Computer Program TWOFNR* (Surrey University version).
[14] R. L. Varner *et al.*, Phys. Rep. **201**, 57 (1991).
[15] M. B. Tsang, J. Lee, and W. G. Lynch, Phys. Rev. Lett. **95**, 222501 (2005).
[16] M. B. Tsang *et al.*, Phys. Rev. Lett. **102**, 062501 (2009).
[17] J. Lee, J. A. Tostevin, B. A. Brown, F. Delaunay, W. G. Lynch, M. J. Saelim, and M. B. Tsang, Phys. Rev. C **73**, 044608 (2006).
[18] J.-P. Jeukenne *et al.*, Phys. Rev. C **1**, 976 (1970).
[19] J. S. Petler, M. S. Islam, R. W. Finlay, and F. S. Dietrich, Phys. Rev. C **32**, 673 (1985).
[20] B. A. Brown, Phys. Rev. C **58**, 220 (1998).
[21] G. J. Kramer *et. al.*, Nucl. Phys. A **679**, 267 (2001), and references therein.
[22] J. Lee *et al.*, Phys. Rev. Lett. **104**, 112701 (2010).
[23] B. M. Sherrill, Prog. Theor. Phys. Suppl. No. **146**, 60 (2002).
[24] D. J. Morrisey *et al.*, Nucl. Instrum. Methods B **204**, 90 (2003).
[25] R. L. Kozub, Phys. Rev. **172**, 1078 (1968).
[26] M. S. Wallace *et al.*, Nucl. Instrum. Methods Phys. Res. A **583**, 302 (2007).
[27] J. Yurkon *et al.*, Nucl. Instrum. Methods Phys. Res. A **422**, 291 (1999).
[28] D. Bazin *et al.*, Nucl. Instrum. Methods Phys. Res. B **204**, 629 (2003).
[29] D. Shapira *et al.*, Nucl. Instrum. Methods A **449**, 396 (2000).
[30] D. Shapira *et al.*, Nucl. Instrum. Methods A **454**, 409 (2000).
[31] J. Lee, Ph.D. thesis, Michigan State University (2010); [http://groups.nscl.msu.edu/nscl_library/Thesis/].
[32] A. Rogers *et al.* (private communication).
[33] Richard B. Firestone and Virginia S. Shirley, *Table of Isotopes*, 8th ed. (Wiley-Interscience, New York, 1998); [http://www.nndc.bnl.gov/].
[34] S. Agostinelli *et al.*, Nucl. Instrum. Methods A **506**, 250 (2003).
[35] F. Lu *et al.* (private communication).
[36] The computer code OXBASH, B. A. Brown *et al.*, MSU-NSCL Report Number 524.
[37] B. A. Brown and W.A. Richter, Phys. Rev. C **74**, 034315 (2006).
[38] A. Signoracci and B. A. Brown, Phys. Rev. Lett. **99**, 099201 (2007).
[39] S. Nummela *et al.*, Phys. Rev. C **63**, 044316 (2001).
[40] D. R. Goosman, P. D. Parker, and A. J. Howard, Nucl. Phys. A **250**, 309 (1975).
[41] R. R. Johnson and R. J. Griffiths, Nucl. Phys. A **108**, 113 (1968).
[42] J. F. Tonn, R. E. Segel, J. A. Nolen, W. S. Chien, and P. T. Debevec, Phys. Rev. C **16**, 1357 (1977).
[43] F. Nunes *et al.* (private communication).